2000-01-2833

Development of high speed spectroscopic imaging techniques for the time resolved study of spark ignition phenomena

C. F. Kaminski, J. Hult, M. Richter, J. Nygren, A. Franke, M. Aldén
Lund Institute of Technology, Sweden

S. Lindenmaier, A. Dreizler, U. Maas
University of Stuttgart, Germany

R.B. Williams
University of Southampton, England

ABSTRACT

This paper reports on the development of novel time resolved spectroscopic imaging techniques for the study of spark ignition phenomena in combustion cells and an SI-engine. The techniques are based on planar laser induced fluorescence imaging (PLIF) of OH radicals, on fuel tracer PLIF, and on chemiluminescence. The techniques could be achieved at repetition rates reaching several hundreds of kilo-Hz and were cycle resolved. These techniques offer a new path along which engine related diagnostics can be undertaken, providing a wealth of information on turbulent spark ignition.

INTRODUCTION

The present paper reports on the application of high speed time resolved spectroscopic imaging techniques using a novel multiple pulse laser facility. The facility allows the application of all standard laser spectroscopic measurement techniques, but at repetition rates reaching several hundreds of kHz. With this equipment it is possible to track dynamic turbulent combustion events in real time with obvious implications for cycle resolved SI-combustion research. The system consists of 4 double pulsed Nd:YAG lasers which can be used either directly or as a pumping source for conventional dye laser systems. A specially designed framing camera is coupled to the laser, capable of taking up to 1 million pictures per second.

In the paper we present a variety of measurements, conducted in purpose built turbulent ignition cells and an SI engine. For the first time, 2D laser spectroscopic imaging techniques could be applied in such systems in a time and cycle resolved fashion. The sample results presented here are part of an ongoing effort to provide a database for detailed models of turbulent spark ignition phenomena.

The paper is organised as follows. In the first part an overview is given on the experimental systems and the spectroscopic imaging techniques developed. Three objects of study are focused on: A constant volume spark ignition cell with a standard fuel injector; a turbulent ignition cell equipped with high speed fans to impart homogeneous isotropic turbulence on the fuel mixture; and finally a 4-stroke laboratory SI-engine.

In the second part we present results obtained from these systems. The techniques are capable of covering nearly the entire phase of combustion in an SI cycle: Here we show results from time resolved measurements of breakdown and subsequent arc phases during the spark event. The ensuing combustion phase could then be examined using either of fuel tracer PLIF, or chemiluminescence spectroscopy.

We furthermore present a novel technique based on the simultaneous application of OH-PLIF and emission spectroscopy, offering additional topological data that neither technique provides on its own.

The techniques presented allow the study of complex reacting flows and turbulence-chemistry interaction in a direct way. Phenomena such as flame kernel development in a turbulent flow and flame extinction can be visualized and tracked in time. We demonstrate the potential of the techniques for engine research, where they may be used to perform cycle resolved measurements of flame front development and air fuel ratio.

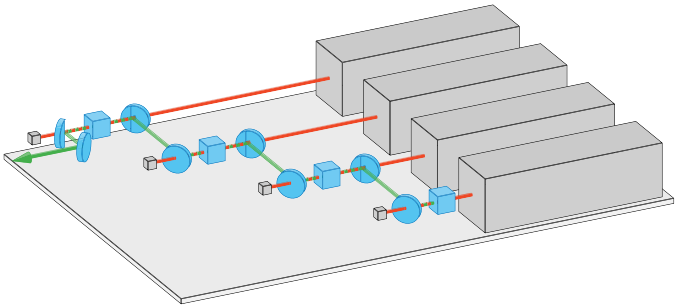

Figure 1: The multiple YAG laser cluster. Round elements signify dichroic beamsplitters which are transmissive for 1064 nm and reflective for 532 nm. Large cubes: Frequency doubling crystals. Small cubes: beam dumps. The single output beam could optionally be doubled to 266 nm by use of an additional, single doubling crystal.

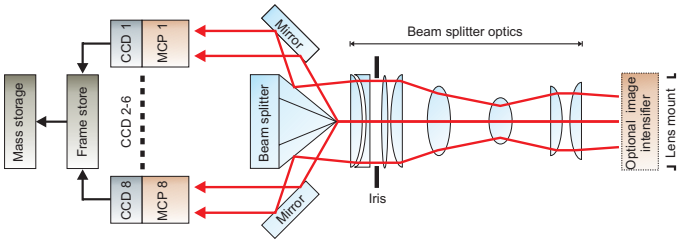

Figure 2: Operating principle of the fast framing camera. MCP: Multi channel plate image intensifier. Light enters from the right, passes internal optics and an iris before impinging on a prism image-splitter. The latter directs individual images onto the MCP's which are sequentially gated.

EXPERIMENTAL

LASER / DETECTOR SYSTEM The high speed spectroscopic imaging system consists of a cluster of 4 Nd:YAG lasers (BMI) which can be fired sequentially at arbitrary repetition rates (with time intervals ranging from ns to about 100 ms between pulses from different cavities) [1]. The output of the lasers is combined using a patented beam combination scheme (BMI) to provide a single output beam. The combination scheme employs a series of dichroic mirrors and successive frequency doubling of the YAG fundamental (at 1064 nm) to achieve beam combination with minimal energy losses (see figure 1). Each oscillator is equipped with a double pulse option (DPO mode) allowing the Pockels cell of each cavity to be switched twice under the duration of the flashlamp pulses. Thus a total of 8 laser pulses can be extracted. Time separations between double pulses from each unit can be chosen to vary between 25 and 145 μs, determined by the length of the flashlamp pulses and the gain build-up times respectively. Pulse energies reaching 600 mJ can be extracted from each cavity in single pulse operation, around 270 mJ are available in DPO mode at the second harmonic (532 nm). As an option a single KDP crystal can be inserted into the output beampath providing radiation at 266 nm, ideally suitable for acetone excitation (see forthcoming sections). The multiple YAG laser cluster can either be used directly (acetone imaging), or, to pump an optional dyelaser (OH fluorescence excitation).

Coupled and synchronised to the laser system is a custom designed version of a commercially available framing camera (Imacon 468, Hadland Photonics, UK). The system features 8 independent intensified CCD detectors (ICCD) with 384 times 576 pixel arrays and 8 bit dynamic resolution. Individual events were imaged onto the individual arrays by use of a Cassegranian prism beam-splitter built into the camera system (see fig. 2). To increase the overall gain of the system and to make it UV sensitive an additional three stage intensifier module was attached to the optical input of the camera prior to the prism beam-splitter. This intensifier could be operated at repetition rates of up to 1 MHz. The electronics of the camera were modified to allow flexible triggering of the intensifiers to arbitrary external events and to synchronise it to the laser system.

EMISSION STUDIES Direct emission was recorded directly by the camera, appropriately filtered for the required measurement task. The camera was triggered directly by the ignition electronics for the two cells used and from a crankshaft encoder (CSE) in case of the engine measurements (see coming sections for more details). Delays between subsequent emission recordings were then triggered internally by the camera hardware. All images recorded here were performed using the optional image intensifier at the camera input (see fig. 2) owing to the weakness of emission signals. Exposure times were matched to the individual situations but typically in the range of 30 to 100μs.

PLANAR LASER INDUCED FLUORESCENCE STUDIES (PLIF) For OH we excited the temperature insensitive $Q_1(8)$ transition of OH in the $A\ ^2\Sigma^+(\mathrm{v}'=1) \leftarrow X\ ^2\Pi(\mathrm{v}''=0)$ electronic band which appears in the 282 nm wavelength region. The exciting laser pulses were obtained using the frequency doubled output from a dye laser (Continuum) operating near 564 nm on Rhodamine 590 dye pumped by the second harmonic (532 nm) of the multiple YAG laser. The laser light was formed into a sheet approximately 50 mm in height and 160 ± 30 μm in width by a cylindrical telescope. A schematic representation of the set-up used for PLIF experiments in the combustion cells is shown in figure 3 and in fig. 6. Subsequent fluorescence in the $\mathrm{v}' = 0 \rightarrow \mathrm{v}'' = 0$ band near 309 nm was directly collected by the appropriately filtered framing camera. Two different modes of operation were employed. In the first mode, 8 excitation pulses were used, and PLIF of OH was recorded by all channels of the camera. In

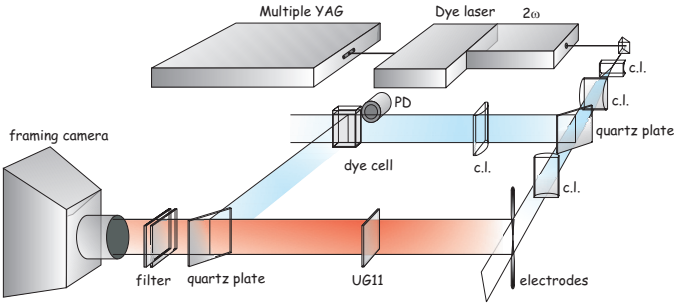

Figure 3: Schematic set-up for the PLIF experiments. 2ω: frequency doubling unit, PD: Photodiode, c.l.: cylindrical lens, UG11: filter to reject laser stray light.

the second mode, we used only four laser pulses and camera channels to record OH-PLIF. In this case, the remaining 4 camera channels were free to record line of sight OH chemiluminescence (direct emission of OH). We gated the camera in such a way that 2 μs after each PLIF image a corresponding OH-chemiluminescence image could be recorded. As will be seen, this approach offers additional structural information on the flame kernel (see discussion further below). The 2 μs time delay is necessary to avoid crosstalk between the channels recording PLIF and chemiluminescence and can be considered instantaneous on the turbulence and overall chemistry time scales prevailing in the studied systems. Exposure times were 200 ns for PLIF and 30 μs for the much weaker emission images.

3-pentanone PLIF The PLIF fuel visualization experiments in the engine were performed with isooctane as a one-component fuel. Since pure isooctane does not show any fluorescence a fluorescent tracer must be added. When choosing a tracer it is of major importance that the tracer follows the fuel during the compression stroke. Hence, the tracer must have physical properties similar to the fuel. For tracing isooctane, 3-pentanone has become a widely accepted dopant. In the presented measurements 5% (v/v) of 3-pentanone has been used as tracer. The low tracer content is not expected to affect the physical properties of the isooctane. For 3-pentanone excitation, 266nm light was used, corresponding to the fourth harmonic of the YAG-lasers. This wavelength is close to the top of the absorption curve and, therefore, the temperature sensitivity is minimized. The spectroscopic properties of the fluorescence from 3-pentanone are almost identical to that from acetone (see below), i.e. a broadband emission ranging from 350-550nm with a peak at 420 nm.

Acetone PLIF For acetone excitation in the fuel injection cell 266 nm light was used, corresponding to the fourth harmonic of the multiple YAG laser. For the combined OH PLIF and acetone PLIF studies the same frequency doubled dye laser operating near 282 nm could be used, since the OH absorption overlaps with acetone absorption bands. Both excitation wavelengths fall within the $S_1, \pi^* \leftarrow S_0, n$ band which extends from about 220 to

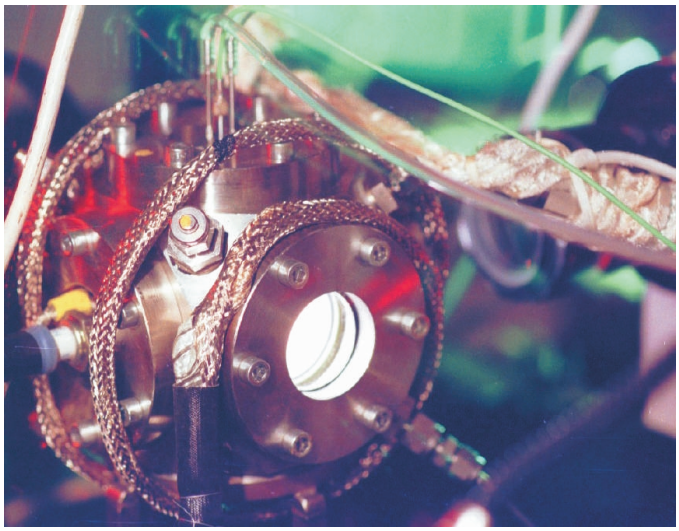

Figure 4: Photograph of the constant volume fuel injection cell used in the present experiments. The spark plug is seen to the left, an ion sensor is seen on the top of the cell. Heating wire was used to preheat the cell.

340 nm. Subsequent fluorescence occurs between 330 and 660 nm with a broad peak around 420 nm [2]. The signals from acetone and OH could thus easily be separated.

COMBUSTION SYSTEMS STUDIED 3 different systems were studied as part of the present work: A constant volume combustion bomb employing a standard port injector and spark ignition system, a fan stirred combustion chamber for premixed homogeneous charges, and a 4-stroke side valve engine.

Fuel injection bomb. For the turbulent acetone PLIF series a constant-volume combustion chamber was used which was designed to ensure that as many parameters as possible were controllable. These included, in addition to standard engine parameters, the mixture homogeneity and the gas flow inside the cell. The chamber had approximately cubic dimensions and a volume of 167 cm^3. It was formed by three orthogonally intersecting cylindrical passages in a cubic block of stainless steel (see fig. 4). Full optical access to the combustion chamber was provided by 3 fused silica windows. A modified spark plug with elongated electrodes was used in the experiments to ensure the laser could come as close as possible to the point of ignition. The cell featured a piezo-electric pressure transducer and an ion current sensor, which could be used to monitor the combustion cycle [3].

A set-up diagram of the system is shown in fig. 5. Direct-acting magnetic valves controlled inlet and outlet of gases. The valves, the ignition system and the PLIF system, as well as the logging of pressure, ion current

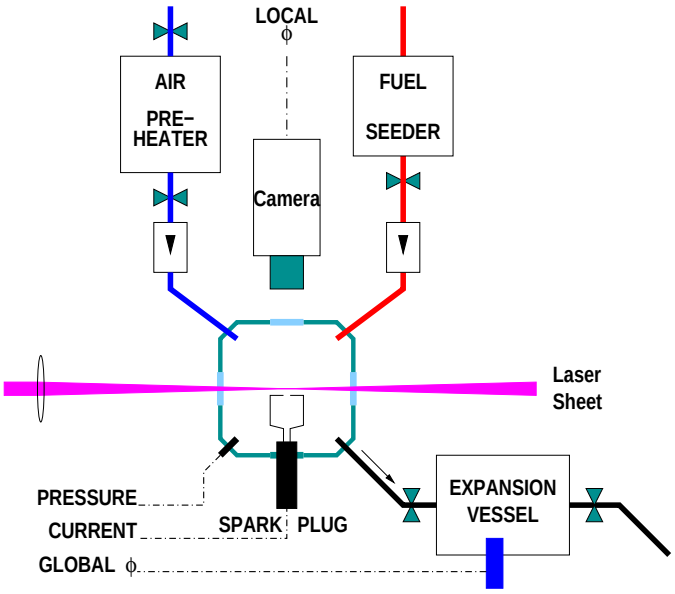

Figure 5: Schematic diagram for the port injection combustion bomb. For details refer to the main text.

and global equivalence ratio, were controlled by a PC by means of a 12-bit A/D card.

Air and fuel were injected separately into the chamber. The air was preheated in an additional vessel to approximately 100 ^{0}C prior to injection. The fuel (methane or propane in the present case) passed an acetone seeder prior to injection. For details refer to fig. 5. A cycle is defined by injection of preheated air, followed by the injection of the gaseous fuel a few milliseconds later. After a user defined delay the mixture is ignited. The length of this delay governs the degree of mixing as well as the amount of turbulence in the cell, which is caused by the injection processes and decays in time. A few seconds after combustion, the outlet valve was opened, and the burned gases allowed to expand into an additional vessel, where an oxygen sensor was used to determine the overall equivalence ratio. The cycle ended with the evacuation of both vessels to a pressure of 20 kPa to ensure a very low EGR. The overall duration of such a cycle amounted to 90 s. Pressure traces were recorded by a flush-mounted, water-cooled, piezoelectric transducer connected to a charge amplifier.

Fan stirred bomb. For the study of turbulent flame growth using OH PLIF a fan stirred combustion bomb was used. Fig.6 shows a schematic drawing of the fan stirred turbulent ignition cell, whose volume measured 55 l. Full details of the system are found in [4]. The following offers only a brief description of the system. Electrodes centered in the cell were made of sharpened tungsten tips, separated by a distance of 1 mm. The cell was filled with homogeneous mixtures of methane and air prior to spark ignition. The mixture could be subjected to controlled degrees of turbulence by adjusting the rotor speed between 0 and 5000 rpm (rotations per minute) effecting

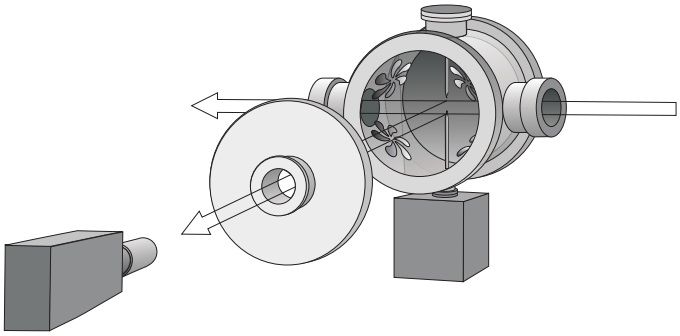

Figure 6: Fan stirred combustion bomb for turbulent ignition studies.

turbulence intensities in the range of 0 to 1.9 ms^{-1} which were measured by LDA (Laser Doppler Anemometry). Spark duration and energy content were controlled by rapid adaptive regulation of the voltage between the electrodes according to the plasma resistance.

SI engine. The test object was a single cylinder, 5 hp, side valve engine (Briggs and Stratton) modified to provide optical access. Since it was of side-valve type, relatively few modifications were required to this end. The original crankcase and piston remained unaltered while the cylinder head was equipped with three quartz windows. For PLIF studies the excitation light passed horizontally through the smaller windows on each side of the combustion chamber whilst signal detection was performed from above (see fig. 7). A photograph of the engine is shown in fig. 8. A crank angle encoder was used to provide trigger signals for the laser and camera systems. In this way the start of the laser pulse train could easily be synchronized to any desired crank angle. Isooctane was used as fuel for the present experiments. Two different types of visualization techniques were performed: a) direct emission recordings of flame kernel chemiluminescence, and b) fuel tracer PLIF. For the latter 3-pentanone was chosen as a tracer for isooctane.

IMAGE PROCESSING To enhance signal to noise ratios in the PLIF images and to simplify image segmentation for subsequent analysis steps we employed an image post-processing scheme based on anisotropic non-linear diffusion filtering [5]. In the present case, we filter the imaged raw data using the equation,

$$\partial_t u = \mathrm{div}(g(|\nabla(G_\sigma * u)|)\nabla u) \qquad (1)$$

where u represents the intensity of the image under consideration, and $g(|\nabla(G_\sigma * u)|)$ represents a locally adaptive diffusive strength. The latter is made proportional to the gradient ∇u in the image itself (after smoothing with a Gaussian kernel G_σ of width σ, which is done for stability reasons [6]). The principle of the method is to smoothen out noise locally by diffusive flow whilst pre-

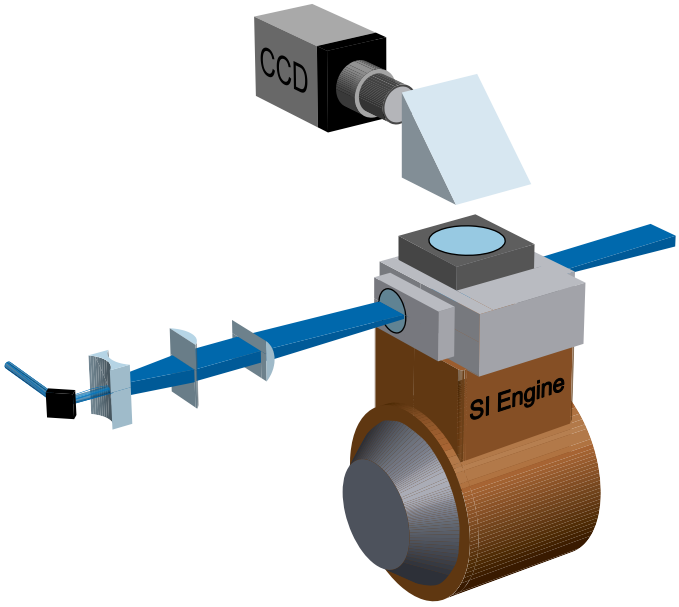

Figure 7: Schematic set-up for engine PLIF experiments. The engine was a 4 stroke engine of side-valve type. The cylinder top was replaced by a quartz disk through which fluorescence and emission signals were recorded. Optical access for the laser was provided by two small side-windows situated near the cylinder top.

venting flow across physically important boundaries. By a proper choice of the diffusion kernel, object boundaries may be enhanced (but need not be, if undesirable) and physical gradients sharpened. Thus determination of object boundaries and image segmentation is greatly simplified.

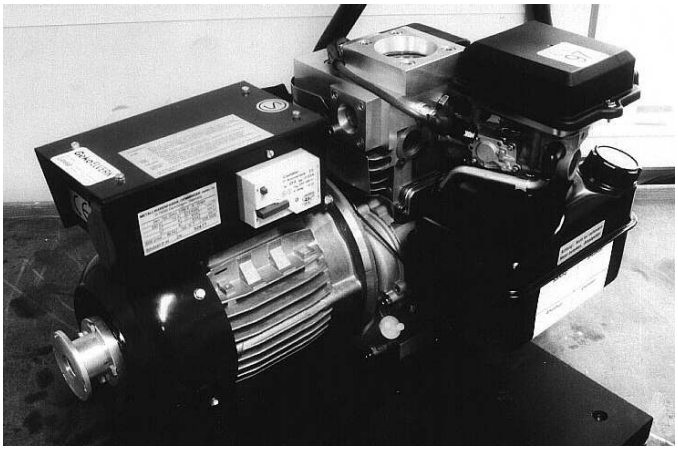

Figure 8: Photograph of the modified 4-stroke engine used for optical diagnostic experiments.

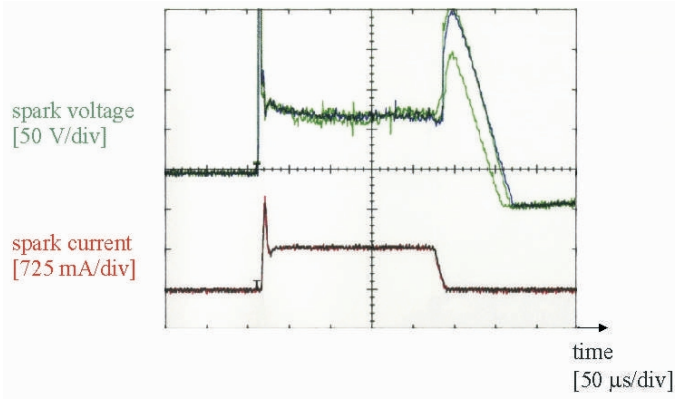

Figure 9: Characteristics of the spark ignition system used in the fan stirred bomb. Traces shown here are three overlaid graphs corresponding to three separate ignition events. Fast high voltage regulation was used to keep the discharge current constant during the discharge phase (lower trace). The upper trace shows the electrode potential during the discharge. The final voltage peak displayed on this trace is irrelevant for spark development. The excellent reproducibility of the discharge is evident from the three current traces shown.

RESULTS

SPARK INITIATION AND BREAKDOWN The combustion vessels described here are subject of modeling activities [4, 7] and the results from measurements as presented here will be used as a database against which models can be compared and validated. For this purpose the ignition systems were designed to be as precisely defined and reproducible as possible. Of major importance was to keep the energy deposited by the spark ignition system as constant as possible from cycle to cycle. In the fan stirred bomb this was achieved by adaptively regulating the voltage drop across the spark gap. In fig. 9 this is shown for three typical ignition events. The top trace shows the voltage drop across the electrode gap as function of time. Two distinct phases can be discerned: The large spike at the beginning effects the breakdown (which at roughly 150 ns is far too short to be seen by the electrode sensor), and the subsequently lower voltage, prevailing for some 200 or so μs, sustains the discharge channel (arc phase). The lower trace displays the plasma current for this discharge which, after the initial breakdown spike, remains constant over the entire event. By adjusting the duration of the discharge, precisely defined energies could be delivered to the combustion system. Nearly the entire energy deposition into the spark occurred during the constant arc phase whose excellent reproducibility is evident from fig. 9.

To provide more detailed information on the discharge process high speed direct emission pictures were recorded. Figure 10 shows consecutive sequences of the breakdown and discharge phases in the fan stirred reac-

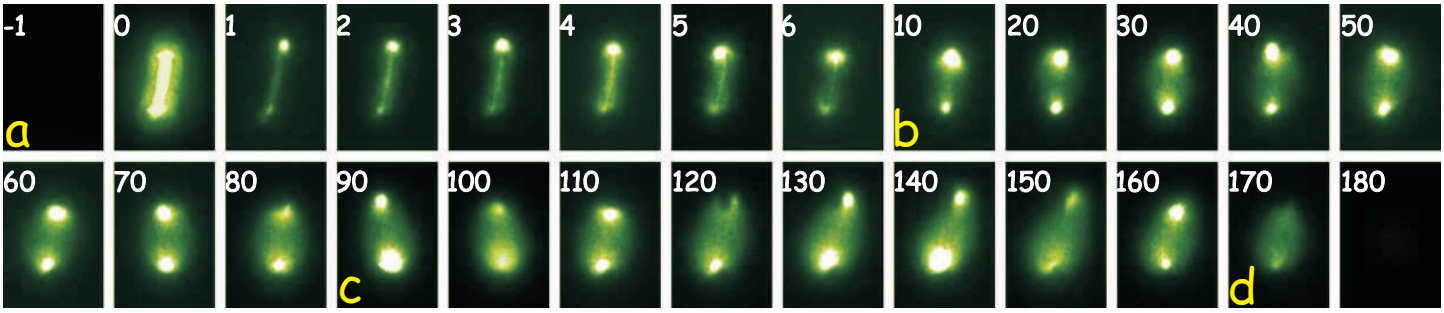

Figure 10: Sequential imaging of a spark ignition event. Numbers in the images correspond to μs after breakdown. Series a-d correspond to 4 discharge events to illustrate the entire sequence of the process.

tor. Four sequences of 8 images each are shown, labeled a-d on the figure (series d features only two consecutive images). Each sequence corresponds to a single ignition event, covering the time interval indicated by the figures in the corners (given in μs relative to the breakdown). The length of the spark channel seen corresponds to 1 mm (distance of the electrodes). The 4 sequences shown are matched to cover an entire spark discharge event. Several features are apparent. During the first 8 images one can follow the buildup of the discharge channel. During breakdown (0μs) the luminous intensity is a maximum, immediately dropping to a very low value after breakdown. One can clearly follow the development and growth of the discharge channel in time. Series a) demonstrates the exquisite sensitivity and time resolution that is afforded by the camera system. Exposure times were only 10 ns for each event covered. Since the signal brightness is several orders of magnitude larger during breakdown the camera gain had to be lowered accordingly on channel 2 to make recording of sequence a) in the figure possible. Since the channel gains can be arbitrarily adjusted on the camera, a dynamic range of several orders of magnitude can be covered within a single time series, something that would be very difficult to achieve with alternative recording devices.

Between about 20 and 170 μs the fully established discharge channel remains almost constant in size. Note how the spark channel is moving in time: In series c) the spark is moving behind the cathode (at 120 μs) leaving a cathode shadow in the image. Such movement of the cathode spot can only be resolved using the fast sequential imaging techniques described here. Note also the development of anode and cathode spots in the series, owing to electric field focussing effects at the sharpened Tungsten tips. Series a) also reveals that the breakdown phase is on the order of ns, much shorter than what the voltage drop across the electrodes may lead to conclude (see fig. 9). The constant overall intensity during the discharge provides further evidence that the energy delivery is constant during this phase.

TURBULENT FLAME GROWTH Following the spark an (initially laminar) flame kernel is initiated in a homogeneous flammable mixture. By subjecting homogeneous methane/air mixtures in the cell to varying degrees of turbulence spark ignition can be studied in a systematic manner over a wide range of parameters such as stoichiometry, spark energy deposition, etc. To provide a good basis for model validation it was chosen to monitor a) flame front topologies and b) concentration fields of combustion generated radicals. Such data is well suited for comparisons with numerical models [7, 8].

Some example results of such runs are shown in figure 11. The imaged area covers approximately 5 cm in height by 6 cm in width. Stoichiometries (ϕ) and rotor speeds (ω in rpm) corresponding to the different series are indicated in the first picture of each series. Time instances are shown below each image. In a) the evolution of the OH concentration field is shown for a stoichiometric laminar flame (fans turned off). In [4] detailed chemical kinetics calculations are presented comparing such flames to laminar flame calculations. Series b) shows the same situation but with weak turbulence levels present ($\omega = 1000$ rpm). One can clearly follow the onset of flame wrinkling. Note also the increase of the flame speed evident from the reduced time difference between consecutive images, since the flame surface is increased by the wrinkling. In c) the same situation is shown as in b) except that the mixture is lean ($\phi = 0.65$). In this case the flame speed is much lower, and the flame is much more strongly wrinkled than the stoichiometric flame in b). Series d) is a flame subjected to high degrees of turbulence, similar to conditions prevailing in typical SI engines. Here $\phi = 1$ and $\omega = 3000$ rpm. The first two images appear black since the flame kernel is initially moving away from the laser sheet. Only in the third picture does the flame reach the laser sheet. The flame is very heavily disturbed by the prevailing turbulence levels. In e) simultaneous emission images are presented corresponding to the series shown in d). The series was obtained in the fashion described in the experimental section. The benefit of these 'simultaneous' line-of-sight recordings is apparent: despite the non-existence of PLIF data in images 1 and 2 of series d) the flame kernel has nevertheless begun to propagate as is clearly evident from the corresponding images in e). The emission signals stem from the entire light emitting flame volume. Combining this data with 2D-PLIF data

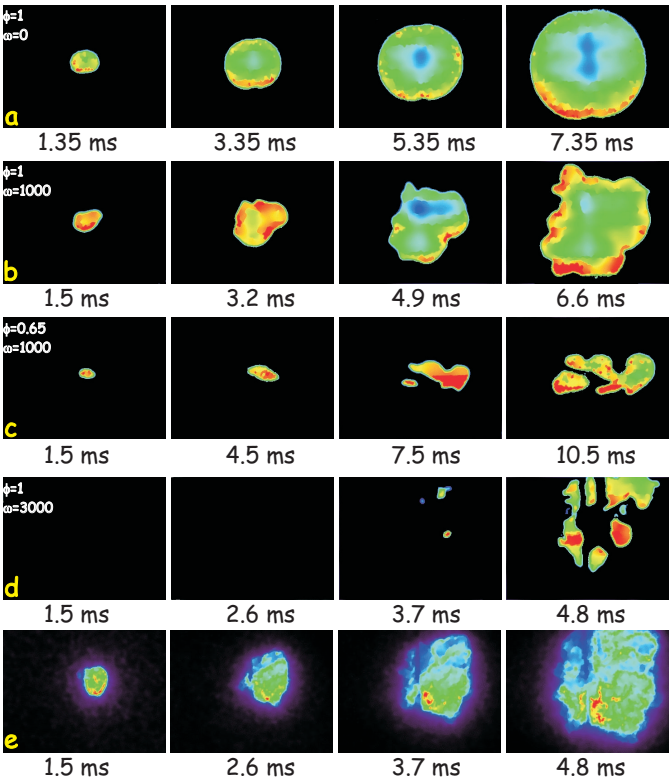

Figure 11: Sequential time resolved imaging of turbulent ignition events by PLIF (series a-d) and chemiluminescence (series e) of OH. Series d and e where taken quasi-simultaneously showing the very different information available from 2D-laser imaging and line of sight integrating techniques. Details are provided in the main text.

both 2 and 3 dimensional aspects of the event are captured. One can think of the PLIF images as a cut through the volume imaged by the line of sight emission technique. A statistical analysis of such topological data is currently being undertaken providing information that neither technique could afford, if applied on its own.

FLAME FRONT TRACKING BY PLIF OF OH AND ACETONE Of major interest to engine research is the capability to provide instantaneous information on the local air/fuel equivalence ratio during combustion, since this has major implications on the efficiency of the process and cycle to cycle variations [9]. Several techniques have been developed for this purpose [10]. A common technique is to tag the fuel with a fluorescing species and to monitor subsequent fluorescence. In the present case we used acetone PLIF to study ignition phenomena in the two cell systems described in the experimental sections. For this purpose the (non-fluorescing) fuels were seeded with acetone which was excited using the same frequency doubled dye laser near 282 nm (see experimental section above). The advantage of the present technique is that the obtained PLIF signals not only are useful to study the local ϕ but also for simultaneously monitoring the flamefront propagation: In regions were temperatures are sufficient to pyrolyse acetone the PLIF signal disappears.

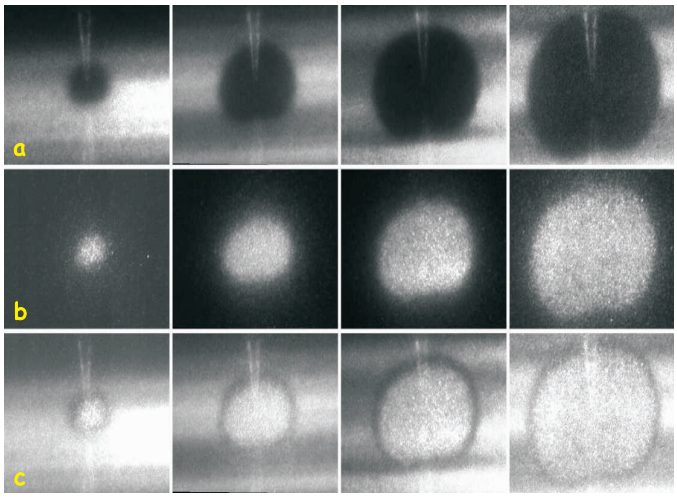

Figure 12: PLIF imaging of acetone (a) and OH (b) as flamefront markers. The lowest row (c) corresponds to both image series superimposed. Note that the regions marked by the two techniques are significantly different.

A question of interest in the present case was how well the acetone contours follow the flamefront as marked by the PLIF-OH images (see fig. 11). For this purpose we recorded OH and acetone image series at simultaneous time positions in the constant volume cell. Fig. 12 shows such sequences for a laminar flame. Series a) corresponds to the acetone signal and b) to OH PLIF. In c) both signals are superimposed. The pictures correspond to unprocessed raw data, the 'stripiness' in the fuel distribution is caused by beam profile variations in the frequency doubled dye laser which were not normalised out (the laser beam propagated at a slight angle with respect to the image plane). The stripes are not present on the much stronger OH signals owing to partial saturation of the signals. Interference from laser scatter was stronger for the acetone images due to lower signal levels, and this is why the electrodes are partially visible on the acetone images.
Note the marked difference between the 'flamefront' radii marked by the two techniques evident from series c). The discrepancy is due to the different temperatures and pressures at which acetone is pyrolysed and OH radicals are produced. Furthermore, the diffusion coefficient for acetone is lower compared to methane [10, 11] although this is to be considered of minor importance in the present situation. In quantitative data extraction for numerical models neglect of these effects could lead to significant problems.

Applied to the port injection system (refer to figures 4 and 5 the acetone PLIF technique can be applied to simultaneously provide information on mixture fraction *and* flame propagation. The image sequence shown in fig. 13 corresponds to a stoichiometric mixture of propane seeded with about 5% of acetone [3]. These pictures were taken with the 4^{th} harmonic of the multiple YAG laser, providing a much more homogeneous beam profile than the frequency doubled dye laser used to obtain the sequences in fig. 12. The fuel residence time (de-

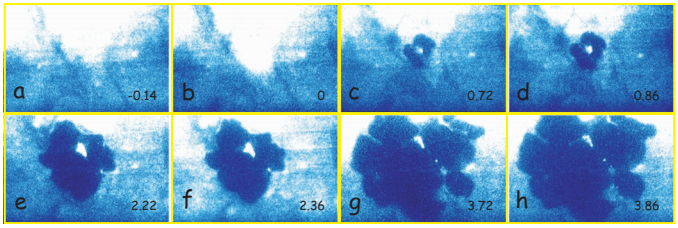

Figure 13: Time resolved PLIF images from the combustion bomb using acetone as a fuel tracer. The acetone signal disappears in burnt regions.

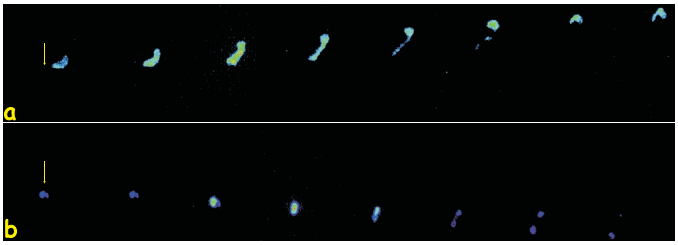

Figure 14: Direct emission images of OH for stoichiometries near the extinction limit. In both sequences shown the time step between successive images is 800 μs. The arrow marks the center between the two electrodes, the imaged region corresponds to 50 by 75 mm. Here $\phi = 0.65, \omega = 2000$.

lay between fuel injection and ignition) in the cell was 50 ms prior to ignition. The results presented here are first results of an ongoing study with the purpose to statistically analyse and correlate flame speeds and flame topology to local stoichiometries and residence times. For residence times > 200 ms nearly laminar flame developments were observed, corresponding to completely homogeneous charges in the combustion chamber. In the presented run one can see that the flame moves towards the fuel richer side at early stages of flame development (seen on images a-d of the sequence where the flame is initially developing into the bright, i.e. fuel rich, regions). Numbers indicated on the images correspond to ms delay after ignition. The imaged region corresponds to about 12 by 18 mm in size.

FLAME EXTINCTION One of the major advantages of the high speed imaging system is its ability to highlight the features of dynamic phenomena in real time and to provide physical insight into their origins. In turbulent diffusion flames the phenomenon of flame extinction could be visualised in real time and in a systematic manner using the present system [12]. In engine research and spark ignition the extinction of turbulent premixed flames is of fundamental interest [8]. The series in fig. 14 capture such an event. They correspond to direct emission recorded with the unfiltered camera for lean ($\phi = 0.65$) homogeneous methane/airmixtures in the fan stirred bomb. Turbulence levels were moderate (0.75 ms^{-1} at $\omega = 2000$ rpm) in both cases shown. The arrows mark the position of the spark gap. Exposure times were 256 μs for each event, owing to the extreme weakness of the signal levels. The

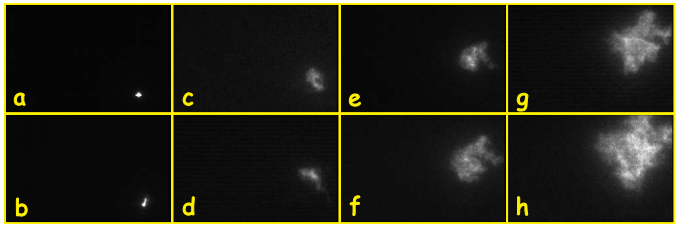

Figure 15: Direct emission (chemiluminescence) images corresponding from the side-valve engine seen in fig.8. In the first image the breakdown of the spark is seen. Exposure times were 30μs, the delay between consecutive images is 250 μs.

time difference between successive images amounts to 800 μs. Clearly one is able to follow the initiation, growth and movement of a small flame kernel in a turbulent field, becoming brighter during the first instances, but then failing to grow and eventually fading away. In series b) a local extinction event can be witnessed (images 6-8). It is caused by turbulent eddies. The turbulence leads to convective transport of reactants towards the flame, building up gradients and thus diffusive loss. As a consequence the loss terms start to dominate over the production terms (radical species, heat generation) and the reactions die out. Fig 14 provides direct evidence of these phenomena.

CYCLE RESOLVED MEASUREMENTS IN PRACTICAL SI ENGINES Finally, we prove that the techniques developed and applied in the laboratory systems described above are directly usable in engine research. The following section describes crank angle resolved measurements of fuel distribution and chemiluminescence. The test object was the single cylinder side valve engine described in the experimental section, operating on isooctane.

Fig. 15 shows cycle resolved chemiluminescence from the engine. The camera was used without filter. In picture a) the breakdown event can be seen and the subsequent flame development can be followed.

The ability to monitor mixture formation and combustion during a single engine cycle can bring major contributions towards the understanding of cycle-to-cycle variations. We demonstrate the capability to make fuel tracer LIF measurements in fig. 16, which shows the fuel distribution during a single combustion cycle. The individual images shown are spaced at 50μs intervals and where obtained using 3-pentanone as the fuel marker (see experimental section for details). Imaging of this type could be combined with imaging of radical species produced during combustion, for example NO concentrations [13] or with OH radical formation as presented in earlier sections of the present paper. Sequential, time resolved imaging, provides unique information on in-cylinder flow-chemistry interactions and has good diagnostic potential for GDI or HCCI applications for example.

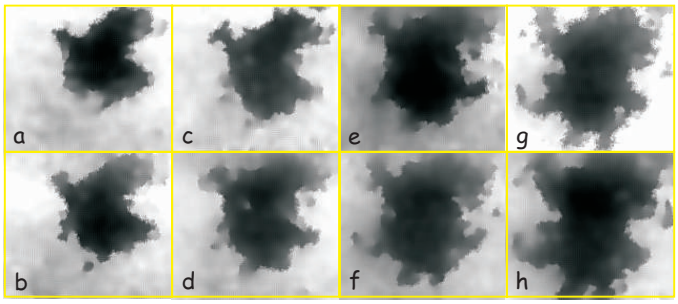

Figure 16: Fuel tracer PLIF from the side-valve engine using 3-pentanone as the fuel marker. Exposure times were 50 ns, the delay between consecutive images is 50 μs. White regions correspond to regions with high fuel concentration, black regions correspond to regions where the mixture is burnt.

CONCLUSION

The present paper reports on a novel way to conduct laser based diagnostic work in spark ignition research in a time resolved fashion. The techniques described offer a wealth of information on the physics and chemistry taking place during turbulent spark ignition and are suited to provide input data for numerical simulations. We have shown results from planar imaging of OH concentrations, and fuel tracer PLIF based on acetone and 3-pentanone. For the first time 2D laser measurements of the flame structure in a real SI engine could be made using these two techniques, time resolved during a single combustion cycle. The diagnostic potential is enormous, with the potential to provide insight into the origins of cycle to cycle variations, yielding more detailed data on spark ignition physics, as well as fundamental data on turbulent flame growth.

REFERENCES

[1] C.F. Kaminski, J. Hult, and M. Aldén. High repetition rate planar laser induced fluorescence of OH in a turbulent non-premixed flame. *Appl. Phys. B*, 68:757–760, 1999.

[2] M.J.G. Borge, J.M. Gigurera, and J.Luque. Study of the emission of the excited acetone vapour at intermediate pressures. *Spectrochim. Acta*, 46A:617–621, 1990.

[3] H. Neij, A. Saitzkoff, R. Reinmann, A. Franke, and M. Aldén. Application of two-dimensional laser-induced fuel tracer fluorescence for ion current evaluation. *Comb. Science. Tech.*, 140(1–6):295–314, 1998.

[4] A. Dreizler, S. Lindenmeier, U. Maas, J. Hult, M. Aldén, and C.F. Kaminski. Characterisation of a spark ignition system by planar laser induced fluorescence of OH at high repetition rates and comparison with chemical kinetic calculations. *Appl. Phys. B*, 70:287–294, 2000.

[5] J. Weickert, B.M. ter Haar Romeny, and M.A. Viergever. Efficient and reliable schemes for nonlinear diffusion filtering. *IEEE Trans. on Image Proc.*, 1998.

[6] F. Catté, P.-L. Lions, J.-M. Morel, and T. Coll. Image selective smoothing and edge detection by nonlinear diffusion. *SIAM J. Numer. Anal.*, 29:182–193, 1992.

[7] C.F. Kaminski, J. Hult, M. Aldén, S. Lindenmaier, A. Dreizler, U. Maas, , and M. Baum. Spark ignition of turbulent methane/air mixtures revealed by time resolved planar laser induced fluorescence and direct numerical simulations. *Proc. Comb. Inst.*, 28, in press.

[8] J. Warnatz, U. Maas, and R.W. Dibble. *Combustion*. Springer, Berlin, 1996.

[9] B. Johansson, H. Neij, M. Aldén, and G. Juhlin. Investigations of the influence of mixture preparation on cyclic variations in an si-engine using laser induced fluorescence. *SAE 950108*, pages 85–99, 1995.

[10] H. Neij. *Development of Laser-Induced Fluorescence for Precombustion Diagnostics in Spark-Ignition Engines*. Ph.D. Thesis, Lund Institute of Technology, 1998.

[11] B. Yip, F.A. Miller, A. Lozano, and R. K. Hanson. A combined OH/acetone planar laser induced fluorescence imaging technique for visualizing combusting flows. *Exp. Fluids*, 17:330–336, 1994.

[12] T. Ding, Th.H. van der Meer, M.Versluis, M. Golombok, J. Hult, M. Aldén, and C.F. Kaminski. *Time-resolved PLIF measurements in turbulent diffusion flames*, volume 3 of *Turbulence, Heat and Mass Transfer*. Aichi Shuppan, Japan, 2000. Y. Nagano, K. Hanjalić and T. Tsui (Eds.).

[13] F. Hildenbrand, C. Schulz, V. Sick, G. Josefsson, I. Magnusson, O. Andersson, and M. Aldén. Laser spectroscopic investigation of flow fields and no formation in a realistic SI engine. *SAE 980148, Journal of Engines*, 107:205–214, 1998.